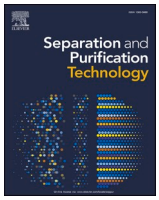
Separation and Purification Technology 366 (2025) 132844



Contents lists available at ScienceDirect

Separation and Purification Technology

journal homepage: www.elsevier.com/locate/seppur





Remediation of acidic effluents from Uranium-Contaminated soil using coffee Residue Biochar: A Combined experimental and Machine learning approach☆

Byung-Moon Jun [a,1], Sung Ho Chae [b,1], Deokhwan Kim [c,d], Changgil Son [e], Tack-Jin Kim [f], Seok Won Hong [g], Yeomin Yoon [h], Kangmin Chon [i], Hojung Rho [c,d,*]

[a] Department of Environmental Science and Engineering, Kyung Hee University, 1732 Deogyeong-daero, Giheung-gu, Yongin-si, Gyeonggi-do 17104, Republic of Korea
[b] School of Environmental Engineering, University of Seoul, 163, Seoulsiripdae-ro, Dongdaemun-gu, Seoul, Republic of Korea
[c] Department of Environment Research, Korea Institute of Civil Engineering and Building Technology (KICT), 283 Goyang-Daero, Ilsanseo-Gu, Goyang-si, Gyeonggi-do 10223, Republic of Korea
[d] Department of Civil and Environment Engineering, University of Science and Technology (UST), 217 Gajeong-Ro, Yuseong-Gu, Daejeon 34113, Republic of Korea
[e] Department of Integrated Energy and Infra system, Kangwon National University, 1, Kangwondaehak-gil, Chuncheon-si, Gangwon-do 24341, Republic of Korea
[f] Radwaste Management Center, Korea Atomic Energy Research Institute (KAERI), 111 Daedeok-Daero 989beon-gil, Yuseong-Gu, Daejeon 34057, Republic of Korea
[g] Center for Water Cycle Research, Korea Institute of Science and Technology (KIST), Seoul 02792, Republic of Korea
[h] Department of Environmental Science and Engineering, Ewha Womans University, 52 Ewhayeodae-gil, Seodaemun-gu, Seoul 03760, Republic of Korea
[i] Department of Environmental Engineering, College of Engineering, Kangwon National University, 1, Kangwondaehak-gil, Chuncheon-si, Gangwon-do 24341, Republic of Korea

ARTICLE INFO

Editor: Dr. B. Van der Bruggen

Keywords:
Biochar
Acidic effluent
Uranium adsorption
Machine learning

ABSTRACT

Uranium contamination resulting from nuclear waste disposal poses significant environmental and health risks, necessitating the development of effective remediation strategies. In this study, we investigate the use of biochar-based adsorbents derived from coffee waste for the removal of U(VI) from acidic effluent produced by real uranium-contaminated soil through acid leaching, providing a novel solution to real-world contamination. Two biochars—pristine and ZnFe-modified—were synthesized, and their U(VI) adsorption performance was evaluated through a comprehensive analysis of their physicochemical properties. The biochar's adsorption performance was assessed under diverse experimental conditions, examining its isotherm, kinetic, and thermodynamic characteristics. Additionally, its behavior was analyzed in the presence of background cations, anions, and humic acid within a real acidic effluent containing U(VI). Despite the significantly larger surface area of ZnFe-modified biochar (1218.4 m^2/g vs. 40.8 m^2/g for pristine biochar), pristine biochar exhibited superior U(VI) adsorption capacity at pH 4. This enhancement was attributed to its negative surface charge, which promotes electrostatic interactions with the positively charged U(VI) ions. Conversely, the positive surface charge of ZnFe-modified biochar hindered U(VI) adsorption efficiency under similar conditions. Machine learning models, including Random Forest, XGBoost, and LightGBM, were employed to predict adsorption capacity and analyze key operational parameters. SHapley Additive exPlanations analysis identified initial uranium concentration, exposure time, and pH as the most critical factors. These findings underscore the novelty of using real uranium-contaminated soil effluent and highlight pristine biochar as an effective, sustainable material for U(VI) removal.

1. Introduction

The use of nuclear energy to satisfy global energy demands has grown owing to its sustainability and cost-effectiveness [1]. Uranium (U) is a critical component of nuclear power production; however, U-containing nuclear waste poses a critical threat to soil condition because it has increasingly returned to soil systems [2,3]. Production of U via mining/milling harm ecosystems due to the improper way to dispose

☆ This article is part of a special issue entitled: 'CESE2024-ICARE' published in Separation and Purification Technology.

* Corresponding author.
E-mail address: hojungrho@kict.re.kr (H. Rho).

[1] Byung-Moon Jun and Sung Ho Chae contributed equally to this work.

https://doi.org/10.1016/j.seppur.2025.132844
Received 3 February 2025; Received in revised form 15 March 2025; Accepted 1 April 2025
Available online 3 April 2025
1383-5866/© 2025 The Author(s). Published by Elsevier B.V. This is an open access article under the CC BY-NC-ND license (http://creativecommons.org/licenses/by-nc-nd/4.0/).

radioactive waste [4]. Moreover, the health risks of uranium to humans are significant owing to its toxicity, which affects the cells, bones, and kidney [5–7]. Thus, proper uranium-removal methods for contaminated waste are required to promote public health sustainability [8,9].

Radioactive waste, including contaminated soil, is produced at various sites, such as electrochemical plant facilities, decommissioned plants, and mineral regions [10–12]. To date, contaminated soil remediation has included either physical separation or chemical extraction methods [12–14]. Physical separation, such as magnetic, attrition scrubbing, and electrokinetic separation, is generally ineffective for elements that are strongly bound to soil particles [14,15]. Chemical extraction methods include the eluent/chelant extraction, use of redox agents, and surfactant-based solubilization [12–14]. Chemical extraction, particularly acid leaching, is an effective method for removing target elements, such as uranium, from contaminated soils [11,16,17]. As an extension of the previous research [18], this study was conducted to treat the waste effluents generated during acid-based remediation. Therefore, we aim to define the scope of this research using the acidic effluent.

Radioactive wastewater containing uranium can be treated using various methods, including (i) physical methods such as membrane separation, evaporation, precipitation, and adsorption, (ii) electrochemical techniques, and (iii) biological methods [17,19–23]. Each method has its own advantages and disadvantages, including environmental friendliness, cost-effectiveness, kinetic properties, byproduct generation, and target selectivity. Among them, adsorption is particularly suitable for treating U(VI)-contaminated water owing to its cost-effectiveness and reusability. Based on the development of novel adsorbents with high adsorption performance, numerous studies have been published on using adsorption to remove U(VI) from real or simulated wastewater [4,24–26].

Biochar-based materials possess numerous oxygen functional groups, exhibit thermal stability and environmental friendliness, and have a porous structure [27–29]. They have been successfully used to treat either real or simulated radioactive U(VI)-contaminated wastewater using adsorption, as presented in approximately 30 published papers [24,25,27–52]. However, these studies lacked insights into the effects of impurities co-leached during acid leaching and did not explore the use of machine learning (ML) to identify key factors influencing uranium adsorption performance, which hinders the development of effective adsorbents for uranium remediation. The practical research scope is different for uranium-contaminated wastewater than that of soil because acidic effluents from uranium-contaminated soil contain high concentrations of impurities, such as Fe^{2+}, Al^{3+}, and Si^{2+}. Notably, only one study has employed ML models to interpret the U(VI) adsorption results using biochar-based adsorbents [46]. From this perspective, the main research question of this study is whether biochar-based materials can effectively treat waste effluents generated from uranium-contaminated soil and yield meaningful results through machine learning analysis.

This study used biochar-based adsorbents for the removal of U(VI) via acid leaching from U(VI)-contaminated soil for the first time. Meanwhile, as referenced in a previous study [53], ZnFe-modified biochar offers the advantages of increased surface area and ease of recovery. If these characteristics can be effectively utilized, it becomes more meaningful from a practical standpoint. Therefore, comparing raw biochar with ZnFe-modified biochar is the novel and significant aspect of this study. Two types of biochar-based adsorbents were synthesized, and their effectiveness in treating U(VI) was compared based on their physicochemical properties. Subsequently, the adsorption performance of the biochar was evaluated under various experimental conditions, revealing its isotherm, kinetic, and thermodynamic properties, and under the presence of background cations/anions and humic acid (HA) in a real acidic effluent containing U(VI). Reusability tests were conducted to elucidate the adsorption–desorption behavior of biochar for practical applications. Furthermore, a feature importance analysis was performed using three types of ML models to elucidate the process mechanisms and optimize the control conditions, offering practical methods to develop eco-friendly ways for remediation of U(VI)-contaminated environments. Finally, a removal mechanism between biochar and U(VI) was proposed, judging from the adsorption results, characterizations, and comparisons with previous researches on U(VI) adsorption using biochar-based materials.

2. Materials and methods

2.1. Evaluation of adsorption and desorption performances

Preparation of biochar-based materials and their characterizations were described in supplementary materials in S1.1 and S1.2, respectively. To treat soil contaminated with U(VI), acid leaching was performed using a 1 M HCl or H_2SO_4 solution with a liquid (acids)-to-solid (soil) ratio of 3:1 with 4 h exposure time. The U(VI)-containing wastewater was recovered via centrifugation, and the solution pH was adjusted by a 1 M NaOH solution. A mixture containing 1,000 and 100 mg•L^{-1} of adsorbent and U(VI), respectively, with 4 h reaction time was used for all the experiments. To elucidate the adsorption isotherms, initial U(VI) concentrations (30, 60, 75, 100, 150, 250, and 350 mg•L^{-1}) were selected. Five recycling tests were conducted using 0.1 M HCl to desorb U(VI) from the as-conducted biochar, and the regenerated biochar was separated via centrifugation.

2.2. Implementing ensemble ML models

This study aimed to implement ML models to classify the biochar-based adsorption capacity (q_e) of U(VI) using experimental data. Three ML algorithms, random forest (RF), extreme gradient boosting (XGBoost), and light gradient boosting machine (LGBM), were employed and compared to determine an optimal model for classifying q_e levels. These models are based on an ensemble (alternatively called tree-based) algorithm and make predictions by collecting each result from a decision tree unit [54]. Although they have the same underlying mechanism, their performance can differ according to the types of target systems (or datasets) to be observed [55–57]. Therefore, the performances of the ensemble models must be investigated to select the best model for classifying q_e levels.

Before model implementation, the input (feature) and target data for the ML models were preprocessed. In this study, the feature and target datasets were preprocessed following the steps introduced in our previous study [58]. Using preprocessing, the feature data had an ordinal format, such as “0,” “1,” “2,” and “3” for 10, 50, 100, and 500 mg L^{-1} background ion concentrations, respectively, while the target data came to range from 0 to 1 due to normalization. Target data ranging from 0 to 1 (normalized target data) were grouped (stratified) into N-class ordinal forms for the classification task of ML models; this step is called “data stratification.” N denotes the degree of stratification, and the target dataset that passed the data stratification contained N data classes. For example, if N was set to five, the target dataset had five integer data: from “1,” corresponding to 0 in a normalized target dataset, to “5” for 1 in the normalized target dataset. During ML modeling, N ranged from 3 to 10 to observe changes in model performance following its variation.

2.3. Shapley additive exPlanation (SHAP) analysis

Among the three ML models, the one with the highest accuracy was selected as the surrogate for feature importance analysis, which determines the influence of input variables on the target variable in ML models. This study conducted a feature importance analysis *via* SHAP. In ML communities, the SHAP analysis is a widely used technique for determining the importance of features. This technique is closely associated with game theory and Shapley values, thereby enabling the interpretation of ML models [59]. The SHAP analysis for ML model classification provides two critical insights: rankings of the total feature

importance and feature performance in individual classes. The ranking of the total feature importance represents the extent to which a specific feature influences the target data, regardless of the data classes or stratification degrees. This attribute indicates the total contribution of an input variable to the target data. However, the feature importance ranking for each individual class reveals how the features affect each class. Thus, a model configured with N data classes results in rankings for N classes. In this study, the effects of the individual features on the target variables were explored using these two rankings.

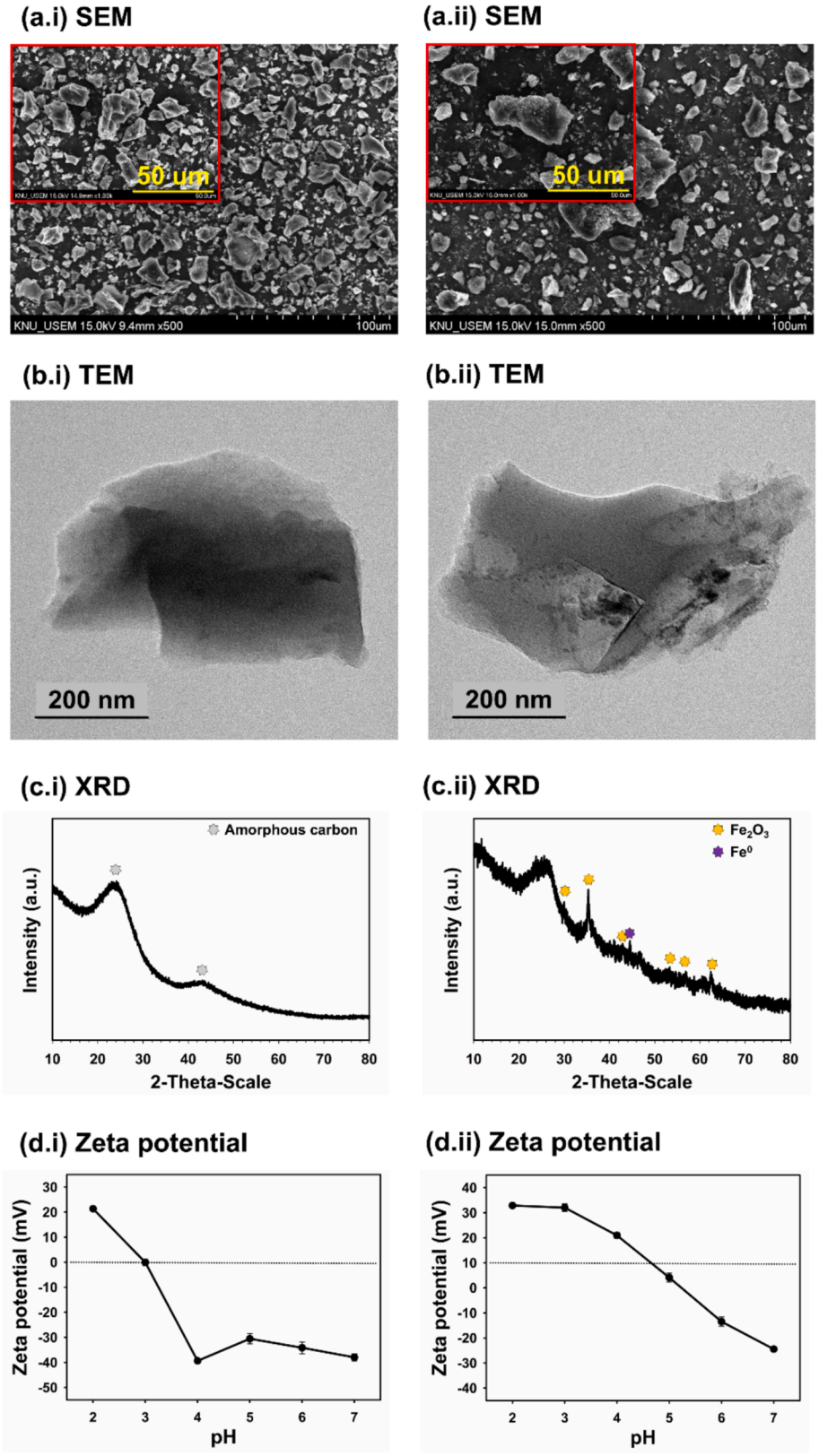


Fig. 1. Various characterizations of the (i) biochar and (ii) ZnFe-biochar in this study: (a) SEM (b) TEM, (c) XRD, and (d) zeta potential.

3. Results and discussion

3.1. Characterization of the biochar-based adsorbents

The micro-morphologies of the pristine and ZnFe-modified biochars were examined using SEM and TEM. The SEM images [Fig. 1(a.i and ii)] revealed that the biochar structures possessed irregular and wrinkled pore shapes. In contrast, the TEM images demonstrated that the biochar structures had smooth surfaces, as illustrated in Fig. 1(b.i and ii). This morphology was consistent with those of several synthesized biochar samples reported in previous studies [27–29,34].

Subsequently, the XRD patterns of both the pristine and ZnFe-modified biochars were recorded and are illustrated in Fig. 1(c.i and ii), respectively. According to the ICDD related to biochar [53], the primary diffraction peaks for biochar appear at approximately 23° and 43°, which are indicative of amorphous carbon. For the ZnFe-modified biochar, the main diffraction peaks were observed at approximately 45°, with additional peaks at 30°, 35°, 43°, 57°, and 63° corresponding to Fe^0 and Fe_3O_4 [53]. These crystallinity results and the dimensions of the biochar-based materials aligned with findings from previous studies [36,37,39,53].

The specific surface area and surface charge of the pristine and ZnFe-modified biochars were confirmed using a porosimeter and zeta potential analyzer, respectively. Determined using the BET method, the specific surface areas of the pristine and ZnFe-modified biochars were 40.8 and 1218.4 $m^2 \bullet g^{-1}$, respectively (Table 1). The pH of the isoelectric point for pristine and ZnFe-modified biochars was approximately 3.0 and 4.5, respectively [Fig. 1(d.i and ii)]. These characterizations were important for this study because both the surface charge and area were key factors in determining q_e [58,60]. Based on these characterizations, we performed adsorption tests using two types of soil washing agents with different pH values to evaluate the effectiveness of U(VI) removal by pristine and ZnFe-modified biochars, as described in Section 3.2.

3.2. Evaluation of the adsorption and desorption properties

3.2.1. Comparison of biochar-based adsorbents under different soil-washing agents

Fig. 2 presents a comparison of the biochar-based adsorbents for the adsorption of U(VI) in four different conditions of wastewater. The adsorption tests used a mixture of 100 and 1,000 mg • L^{-1} of U(VI) and

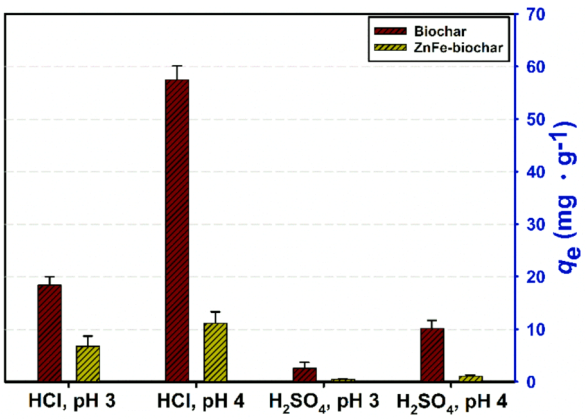


Fig. 2. Comparison of biochar-based adsorbents for the adsorption of U(VI) in four different types of wastewater.

biochar with a 4 h reaction time. In every experiment, the pristine biochar exhibited a higher q_e than the ZnFe-modified biochar. This observation aligned with the interpretation of Fig. 1(d.i and ii), indicating that the surface charge was a crucial factor in determining the adsorption performance of the biochar for U(VI) removal. Furthermore, using HCl as a soil-washing agent resulted in a higher q_e value for both types of biochar at pH values of 3 and 4 compared to H_2SO_4. This finding supported the significance of electrostatic attraction as a primary mechanism for U(VI) removal by the adsorbents. For example, the interruption of electrostatic interactions resulted from competitive interactions between the negatively charged biochar and divalent sulfate anions [58,61]. Moreover, small amounts of U(VI) were captured even though the biochar had an almost neutral surface charge at pH 3 [Fig. 1 (d.i)]. The surface complexation between U(VI) and the O/N functional groups of the biochar could have occurred [36,49], facilitating the removal of U(VI). Therefore, pristine biochar and HCl (at pH 4) were selected as the adsorbent and soil-washing agent, respectively, for subsequent U(VI) treatment in the following sections.

3.2.2. Isotherm, kinetic, and thermodynamic studies

The adsorption isotherms were elucidated by examining the adsorption performance relative to the initial adsorbate concentration

Table 1
Comparison of adsorption capacity for U(VI) by biochar used in this study and by reported biochar-based adsorbents.

Adsorbent	Surface area ($m^2 \bullet g^{-1}$)	Parameters	Adsorption performances ($mg \bullet g^{-1}$)	Models	Ref.
Ash-poor corn cob biochar	>500	*Sorbent* = 2,500 mg•L^{-1} U(VI) *Con.* = 25 mg•L^{-1} pH = 6.0	163.0 (*Maximum*)	Pseudo-second-order kinetic Langmuir	[45]
Iron oxide-rice husk biochar	109.7	*Sorbent* = 200 mg•L^{-1} U(VI) *Con.* = 60 mg•L^{-1} pH = 4.0	52.6 (*Maximum*)	Pseudo-second-order kinetic Langmuir	[51]
Si-biochar@Fe	62.9	U(VI) *Con.* = 0.5 mg•L^{-1} pH = 6.0	138.9 (*Maximum*)	Pseudo-second-order kinetic Langmuir	[24]
δ-MnO_2 modified biochar	550.8	*Sorbent* = 500 mg•L^{-1} U(VI) *Con.* = 50 mg•L^{-1} pH = 5.0	61.5 (*Maximum*)	Pseudo-second-order kineticFreundlich	[34]
Iron oxide-bamboo biochar	129.8	*Sorbent* = 1,000 mg•L^{-1} U(VI) *Con.* = 300 mg•L^{-1} pH = 4.5	70.5 (*Equilibrium*)	Pseudo-second-order kinetic Langmuir	[38]
Biochar	40.8	*Sorbent* = 1,000 mg•L^{-1} U(VI) *Con.* = 100 mg•L^{-1} pH = 4.0 (HCl)	57.5 (*Equilibrium*)	Pseudo-second-order kinetic Langmuir	This study
Biochar	40.8	*Sorbent* = 1,000 mg•L^{-1} U(VI) *Con.* = 350 mg•L^{-1} pH = 4.0 (HCl)	96.3 (*Equilibrium*)	Pseudo-second-order kinetic Langmuir	This study
ZnFe-biochar	1218.4	*Sorbent* = 1,000 mg•L^{-1} U(VI) *Con.* = 100 mg•L^{-1} pH = 4.0 (HCl)	11.2 (*Equilibrium*)	–	This study

[61]. Fig. 3 illustrates the isotherm study of biochar for U(VI) over an initial concentration range of 30–350 mg•L^{-1}. The adsorption capacity q_e of U(VI) onto the biochar increased with the initial concentration of U (VI). The Isotherm models were utilized to assess the homogeneous and heterogeneous surface adsorption [61], as depicted in the inset images of Fig. 3. The Langmuir model exhibited a higher correlation coefficient ($R^2 = 0.993$) than the Freundlich model ($R^2 = 0.984$), indicating that U (VI) adsorption onto the biochar was consistent with monolayer coverage. Previous studies reported similar results for the Langmuir isotherm model of the biochar-based adsorption of U(VI) [24,32,37,51].

Adsorption kinetics are crucial for determining the optimal and practical operation conditions [4]. The impact of exposure time on the adsorption of U(VI) by biochar was assessed over 0–1,440 min, as depicted in Fig. 4. Notably, the adsorption reached equilibrium within 240 min. The inset images in Fig. 4 present the results of the various kinetic models used to elucidate the mechanism of U(VI) adsorption by biochar. Among them, the pseudo-second-order model exhibited the highest correlation coefficient ($R^2 = 0.999$), outperforming the pseudo-first-order ($R^2 = 0.865$), Elovich ($R^2 = 0.934$), and intraparticle diffusion models ($R^2 = 0.784$). Therefore, the adsorption process of U(VI) by biochar was predominantly governed by chemisorption [58,62]. This finding aligned well with other studies that investigated U(VI) adsorption using biochar-based adsorbents [25,31,38,48,50]. The kinetic parameters for U(VI) adsorption by biochar that were derived from these models are summarized in Table S1.

The influence of temperature on U(VI) adsorption by biochar was investigated over the temperature range of 293–313 K. The q_e of U(VI) by biochar was 57.5, 59.3, and 60.2 mg• g^{-1} at 293, 303, and 313 K, respectively. The ΔG values for U(VI) were − 0.74, −0.95, and − 1.08 kJ• mol^{-1} when the solution temperature was 293, 303, and 313 K, respectively (Table S2). Moreover, the ΔH and ΔS values for U(VI) were 4.24kJ• mol^{-1} and 0.02kJ• mol^{-1} K^{-1}, respectively, indicating that the adsorption process was both spontaneous and endothermic process and that randomness increased as the temperature increased (Table S2). These findings were consistent with those of previous studies on the adsorption of U(VI) by biochar-based adsorbents [29,36,43,48].

3.2.3. Effect of co-cations/anions and HA on adsorption

The effects of background ions and natural organic matter (NOM) on the adsorption capacity q_e of U(VI) by biochar were evaluated to determine the key parameters for effective adsorption, with a focus on engineering and practical applications. Common background solutions, such as NaCl and $MgCl_2$, were evaluated at concentrations ranging from 50 to 1,000 mg • L^{-1}. Additionally, based on previous studies, iodide ions and HA were chosen as examples of radioactive background co-cations/anions and NOM, respectively [58,63]. Fig. 5 illustrates the influence of background co-cations/anions and HA on U(VI) adsorption by biochar. Notably, varying the NaCl and NaI concentrations from 50 to 1,000 mg • L^{-1} minimally impacted the adsorption capacity q_e of U(VI), despite the occurrence of electrostatic shielding between U(VI) and biochar due to the increased ion concentrations [64]. For $MgCl_2$, the q_e of U(VI) slightly decreased from approximately 58 to 52 mg • g^{-1}, which was likely due to competition between U(VI) and Mg^{2+} [61]. In contrast, HA, which carries a negative charge under mildly acidic conditions, enhanced the electrostatic interaction between the biochar and U(VI), as depicted in Fig. 5. Experimental findings with H_2SO_4 as the acidic agent (Fig. 2) showed that the hydrophobic aromatic structure of HA enhanced π–π interactions with biochar, thereby enhancing the adsorption of both U(VI) and biochar. Thus, the decreased net positive surface charge improved the removal efficiency of U(VI) by biochar and HA, which aligned well with the results of previous studies [61,65]. The mechanism driving U(VI) removal was primarily attributed to electrostatic interactions, as evidenced by the influence of cations and HA on U(VI) removal.

3.2.4. Sequential adsorption–desorption cycles

The reusability of adsorbents is a critical parameter from a practical standpoint [53]. To assess the regeneration capability of the biochar, 0.1 M HCl with a 1h reaction time was used to elute U(VI). This approach was based on the observation that biochar showed extremely low removal performance at less than pH 3 (Fig. 2) and had a positive surface charge <pH 3.0 [Fig. 1(d.i) and 1(d.ii)]. Fig. S1 shows the results of the five sequential adsorption–desorption cycles for U(VI) removal. The adsorption capacity q_e of U(VI) by biochar decreased from 57.5 to 50.3

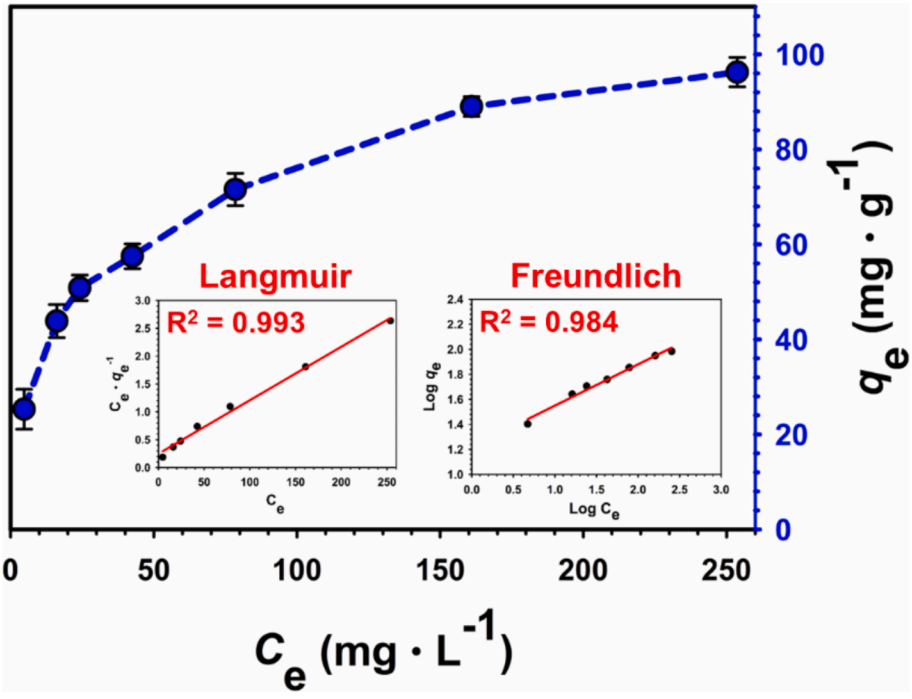


Fig. 3. Isotherm analysis of U(VI) adsorption relative to exposure time. Inset figures demonstrate the findings of isotherm models to interpret U(VI) adsorption by biochar.

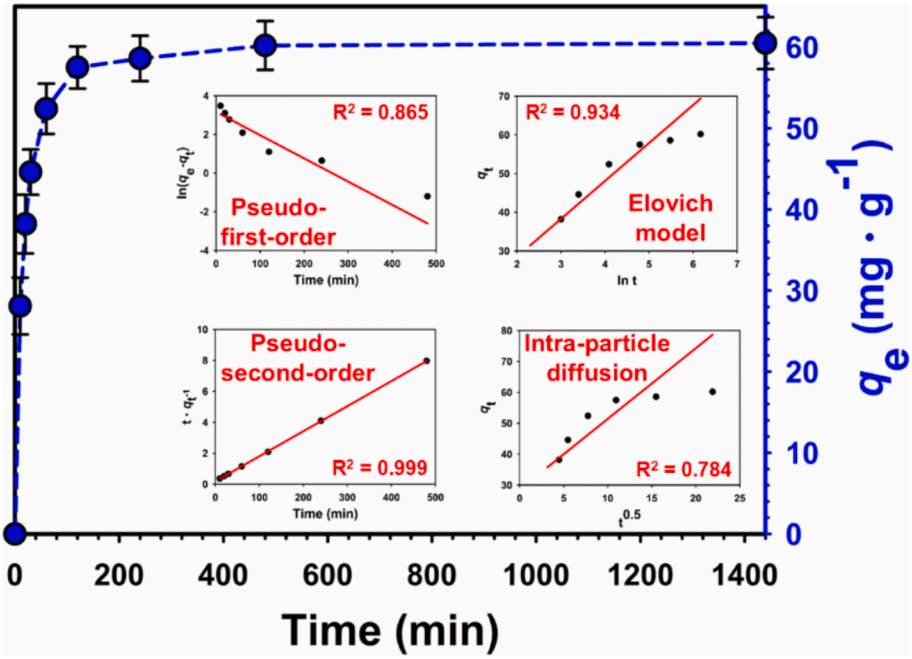


Fig. 4. Kinetic analysis of U(VI) adsorption relative to exposure time. Inset figures demonstrate the findings of kinetic models to interpret U(VI) adsorption by biochar.

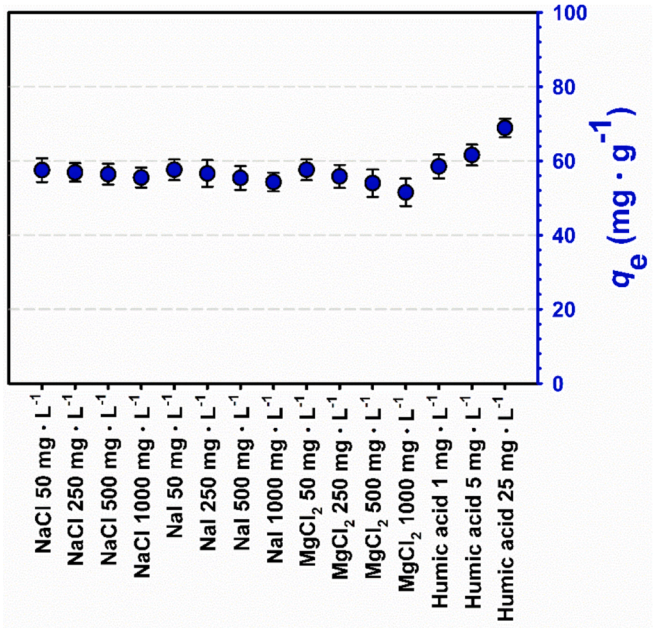


Fig. 5. Influence of co-cations/anions and humic acids on U(VI) adsorption by biochar.

mg • g^{-1} over the five adsorption/desorption cycles. This slight reduction in q_e indicated that the biochar maintained a reasonable and comparable reusability performance to other biochar-based adsorbents [24,30,37,40,44], rendering it suitable for removing U(VI) in real wastewater applications.

3.3. Selecting the optimal ML classification model

Using the biochar experimental data, the ML classification models were trained and tested with a dataset split of 70 % and 30 % for training and testing, respectively. Each dataset was shuffled 100 times with different random seeds for each model and classification-degree pairs to ensure robustness. The final model performance was determined by averaging the results obtained from all the random seeds. Two performance metrics for the ML models, prediction accuracy (PA) and F1-score (F1), were used because they represent the accuracy of an ML classification model. However, F1 is often preferred for imbalanced datasets with uneven class distributions [66]. Thus, this study simultaneously considered PA and F1 for a detailed comparison of the model performances. Fig. 6 illustrates the performance variations of the ML classification models employed in this study: red, blue, and green for RF, XGBoost, and LGBM, respectively. As shown in Fig. 6a, the PA values of the ML models gradually decreased as the stratification degree (N) increased and temporarily increased only when N was set to 6. This increase was attributed to the distribution of the target dataset for N = 6, in which most of the data points belonged to a specific class (Fig. S2 and Section S2.1). Moreover, this temporary increase in accuracy at N = 6 resulted in a sharp decrease in performance at N = 7 in most models (Table S3). Therefore, lower degrees of stratification were generally better for model performance based on PA. Fig. 6b also presents similar trends for F1.

Among the models, RF consistently outperformed the others, achieving the highest accuracy in terms of both PA and F1. This superior performance was consistent with that of a previous study on U(VI) adsorption [58], supporting RF as the most suitable model for this system. Conversely, LGBM exhibited the lowest performance for both PA and F1 among the three models selected in this study. In particular, the F1 values of LGBM were significantly lower than those of the other models (Fig. 6b). The significant difference in performance between RF and LGBM underscores the importance of model comparison when selecting an optimal ML model for a specific purpose, even when the underlying algorithms share similarities. Table S3 summarizes the results of the ML model implementation. RF with N = 3 was the most appropriate model and degree of classification for the U(VI) adsorption system; therefore, it was selected as the final model for further analysis. The contributions of the features to the target data (q_e) were subsequently examined using the SHAP analysis.

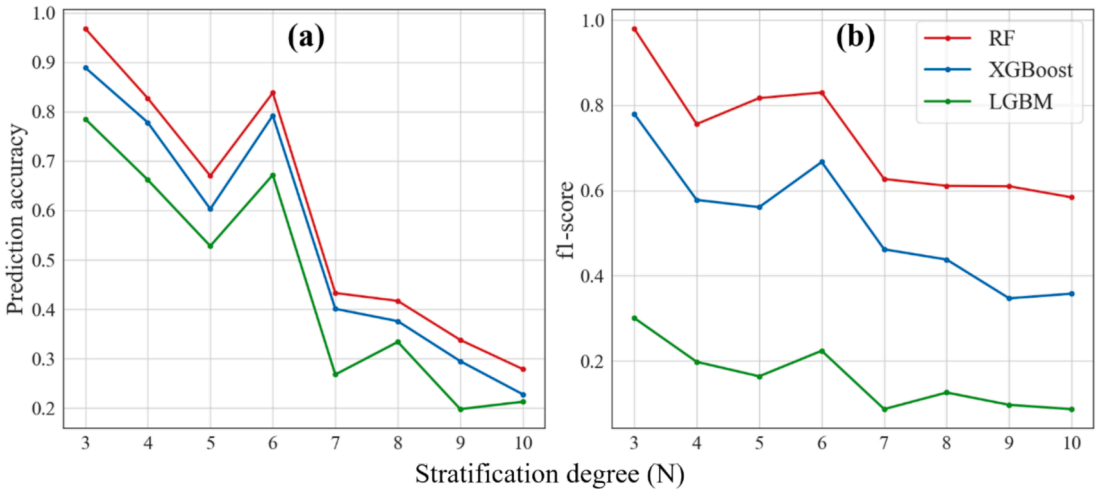


Fig. 6. The performance variation of implemented ML classification models in terms of (a) prediction accuracy (PA) and (b) f1-score (F1): note that RF (red), XGBoost (blue), and LGBM (green) stand for the random forest, extreme gradient boosting, and light gradient boosted machine, respectively.

3.4. *Feature importance analysis using SHAP*

An RF model with N = 3 was applied to the SHAP analysis to investigate the feature contributions to the predicted q_e levels of the biochar-based materials. In this study, the feature data used for the SHAP analysis were subjected to the variable inflation factor (VIF) test to ensure the absence of multicollinearity. As a result, all features employed in this study were found to have low VIF values (VIF < 2), confirming low multicollinearity; see S2.2 and Table S4. Fig. 7 illustrates the SHAP analysis results, illustrating the weights of the individual features to q_e. In Fig. 7a, the ranking for the total feature importance is depicted with "mean (|SHAP value|)" on the horizontal axis. A larger mean (|SHAP value|) indicates that a feature has a greater effect on the target data. The total feature importance ranking illustrated in Fig. 7a was segmented into three categories corresponding to the different levels of normalized q_e: dark pink for low q_e (0 ≤ normalized target data < 1/3), blue for modest q_e (1/3 ≤ normalized target data < 2/3), and olive for high q_e (2/3 ≤ normalized target data ≤ 1). As illustrated in Fig. 7a, the initial uranium concentration (U conc.) was the most influential feature, followed by exposure time and organic concentration. Thus, the q_e level was primarily determined by "U conc." and "exposure time" with respect to the overall dataset. However, the feature importance rankings in individual classes were significantly different. "Exposure time" became the most influential feature for the

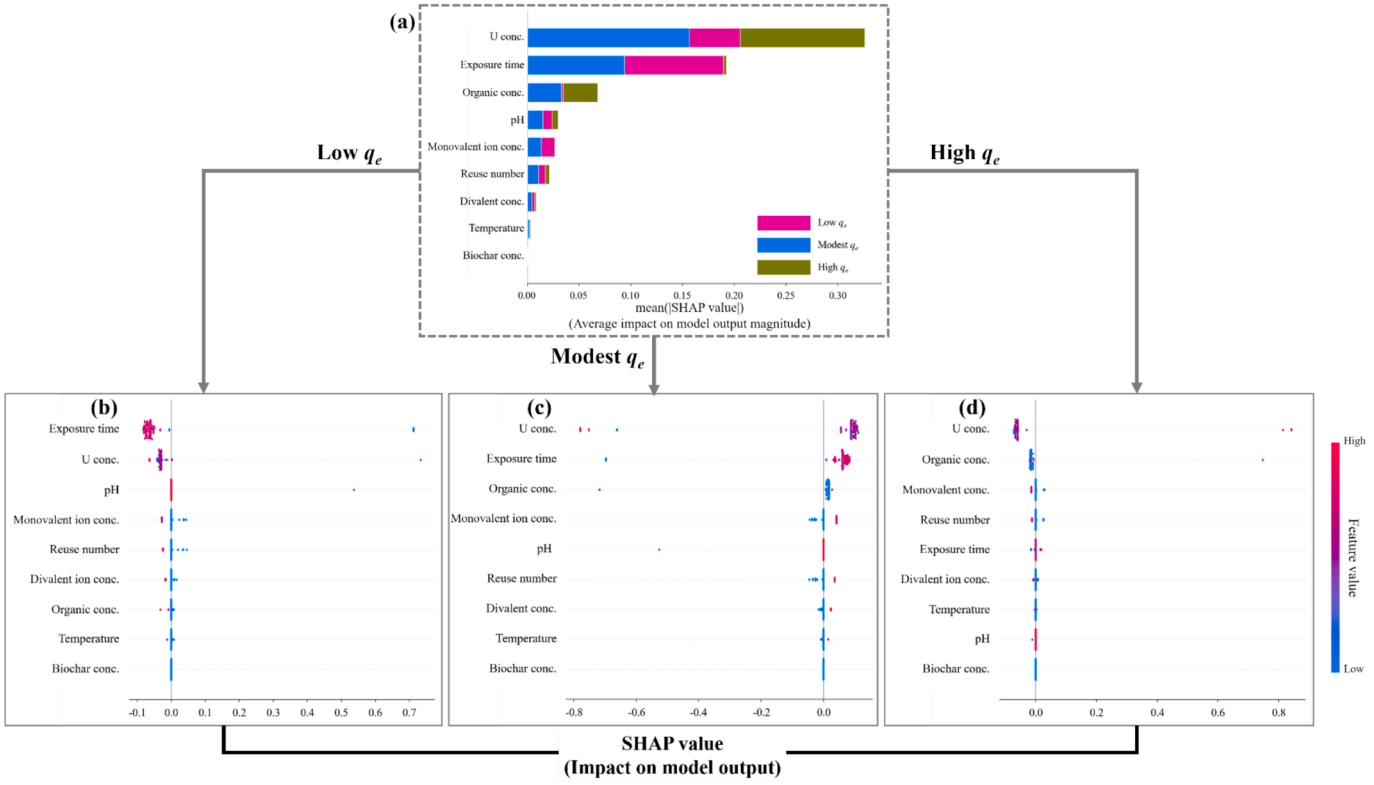


Fig. 7. The results of Shapley additive explanation (SHAP) analysis: (a) a figure illustrating a ranking for the total feature importance; ranking for the features' importance in the (b) 'low q_e level,' (c) 'modest q_e level,' and (d) 'high q_e level' classes.

low q_e while "U conc." maintained its dominance at modest and high q_e levels (individual bars in Fig. 7a). This variation highlighted the dynamic relationship between the features and their impact on different adsorption levels. Other features, such as monovalent ion concentration and pH, also shifted in importance across the different classes, underscoring the need to contextually consider feature importance. Fig. 7b–d provide a more detailed view of the influence of each feature on the model output classes. Unlike that shown in Fig. 7a, several groups of dots represent the impact of each feature on the q_e levels. The dots shown in Fig. 7b–d correspond to data points, and their colors indicate the actual magnitude of the feature data value (color bar on the rightmost side). As the value of the feature data increased, the dots turned red (positive feature data), whereas the color turned blue when it decreased (negative feature data). The correlation between each feature and target data could be understood based on this attribute. For example, if a red dot was on the positive side of the horizontal axis (SHAP value), it could be interpreted as "the target data increased when the feature value was high." In this case, the features and target data were positively correlated. Conversely, the feature and target data were negatively correlated if the dot was red and on the negative side of the horizontal axis. This concept could also be applied to the blue color. Moreover, "exposure time" considerably contributed to lowering the q_e level by exhibiting a strong negative correlation with the low q_e (Fig. 7b). "U conc." also exhibited a strong influence on low q_e with a middle (purple) negative correlation. In contrast, the complexion of the modest q_e was completely opposite to that of the low q_e (Fig. 7c). "U conc." was selected as the most influential feature and exhibited a moderately positive correlation with the q_e level. "Exposure time" was also positively correlated with the modest q_e, unlike the low q_e. For the high q_e, "U conc." became the only high-impact feature because "exposure time" marked the fifth place. Except for "U conc." and "exposure time," the other features negligibly impacted the target data. Only "organic conc." contributed slightly to the modest and high q_e levels.

The results of the SHAP analysis implied that feature importance rankings could vary greatly depending on the viewpoint. Moreover, an analysis such as that represented in Fig. 7a would be sufficient to interpret an overall system. However, in-depth analyses are required, and point-by-point investigations, such as those shown in Fig. 7b–d, must be executed to understand the detailed feature contributions to each class. Therefore, researchers should determine the appropriate depth of analysis based on study objectives to provide comprehensive and meaningful insights.

3.5. Adsorption mechanism

The adsorption mechanism of U(VI) by biochar was proposed based on the experimental results and further characterization, including FTIR and XPS analyses, of the pristine and ZnFe-modified biochars (Fig. 8). Since our institute (Korea Atomic Energy Research Institute) was limited to removing samples from radiation-controlled areas, we could not consider FTIR and XPS analyses before and after the reaction. Thus, our proposed adsorption mechanism between biochar and U(VI) was based on (i) the differing experimental results between the pristine and ZnFe-modified biochars, (ii) adsorption performances under various conditions, (iii) pristine characterizations, and (iv) correlation with previous studies.

First, the pristine and ZnFe-modified biochars were successfully synthesized, as demonstrated by the FTIR and XPS analyses (Fig. 8).

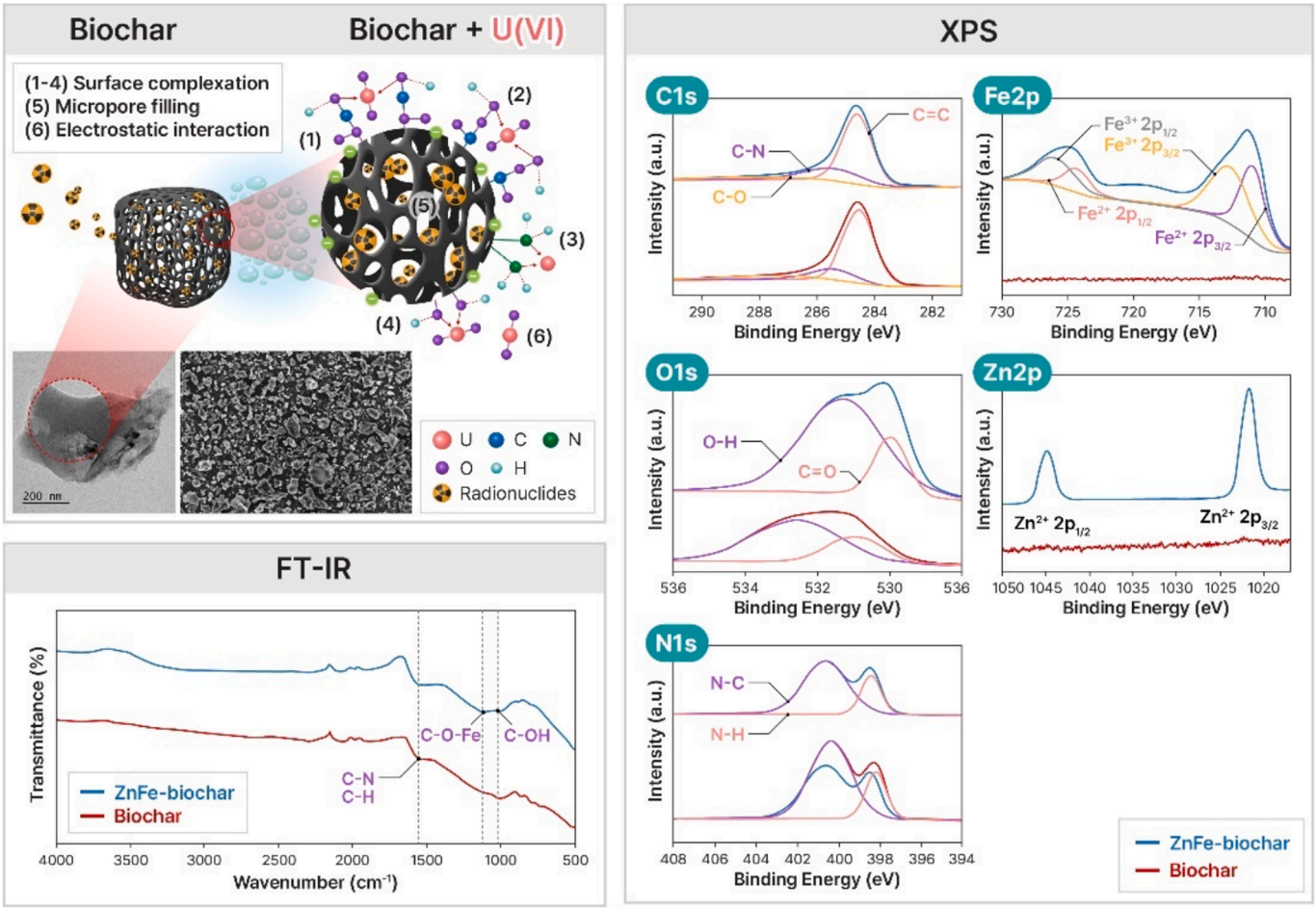


Fig. 8. Proposed mechanism for U(VI) adsorption by biochar-based adsorbents.

Biochar comprises carbon-based substrates with O/N functional groups, including C–N, C–O, C=O, N–H, N–C, and O–H bonds. As illustrated in Fig. 2, pristine biochar consistently demonstrated a higher q_e than ZnFe-modified biochar, even though the surface area of ZnFe-modified biochar is 30 times larger than that of pristine biochar. Thus, micropore filling and a larger surface area were not the primary factors determining the adsorption mechanism between U(VI) and biochar; rather, electrostatic interactions were the primary contributors [Fig. 1(d.i and ii)]. This was demonstrated by the significant decrease in q_e due to the hindrance of electrostatic attraction when H_2SO_4 was used as a soil-washing agent, as well as by the desorption properties observed under acidic conditions (0.1 M HCl). Even though the surface charge of the biochar was nearly neutral at pH 3, small amounts of U(VI) were still captured [Fig. 1(d.i) and 2]. Therefore, surface complexation likely occurred between U(VI) and the O/N functional groups in the biochar. Several studies have described the adsorption mechanism through O/N functional group-based surface complexation using FT-IR and XPS analyses, further supporting our hypothesis [28,36,42,43,49,51]. In conclusion, the primary adsorption mechanism for U(VI) capture by biochar was driven by electrostatic interactions, while surface complexation and micropore filling played minor roles, as summarized in Fig. 8.

4. Conclusions

In this study, pristine and ZnFe-modified biochars were used to investigate the adsorption mechanism of U(VI). The microstructures of both biochars were examined using SEM and TEM for morphology and XRD for crystallinity. The adsorption behavior of pristine biochar followed pseudo-second-order kinetics and the Langmuir isotherm model based on the influence of contact time and initial U(VI) concentration on q_e, respectively. Furthermore, the adsorption process was spontaneous and endothermic, with increasing randomness as temperature increased. To better understand the process and optimize the experimental conditions, a further analysis using ML models (RF, XGBoost, and LGBM) was successfully performed, revealing the relationship between the adsorption performance and several parameters. Finally, the primary removal mechanism of U(VI) on biochar was proposed by integrating the experimental differences between pristine and ZnFe-modified biochar, the adsorption performance across different conditions, material characterization, and comparisons with previous studies. The surface charge was identified as a key factor in determining the adsorption capacity (q_e). Table 1 presents a comparison of the U(VI) adsorption capacities of the biochars used in this study and previously reported biochar-based adsorbents. Our study indicates that biochar is an effective material for U(VI) removal from wastewater because the q_e values were comparable to those of other adsorbents, even when accounting for the surface area differences among the materials. Meanwhile, based on previous studies, evaluating practicality through research related to energy analysis, life cycle assessment, and emissions social cost would be a highly relevant topic for future studies [67–70].

CRediT authorship contribution statement

Byung-Moon Jun: Conceptualization, Writing – original draft, Investigation, Validation. **Sung Ho Chae:** Writing – original draft, Methodology, Investigation. **Deokhwan Kim:** Methodology, Investigation. **Changgil Son:** Validation, Investigation. **Tack-Jin Kim:** Writing – review & editing, Project administration. **Seok Won Hong:** Writing – review & editing. **Yeomin Yoon:** Writing – review & editing. **Kangmin Chon:** Writing – review & editing. **Hojung Rho:** Conceptualization, Project administration, Supervision, Funding acquisition, Writing – review & editing.

Declaration of competing interest

The authors declare that they have no known competing financial interests or personal relationships that could have appeared to influence the work reported in this paper.

Acknowledgements

This work was supported by the Korea Institute of Energy Technology Evaluation and Planning (KETEP) and the Ministry of Trade, Industry & Energy (MOTIE) of the Republic of Korea (20224000000260). This research was also supported by the Nano & Material Technology Development Program through the National Research Foundation of Korea (NRF) funded by the Ministry of Science and ICT (No. RS-2024-0044094).

Appendix A. Supplementary material

Supplementary data to this article can be found online at https://doi.org/10.1016/j.seppur.2025.132844.

Data availability

Data will be made available on request.

References

[1] H.-K. Lee, B.-M. Jun, I. Kim, H.-C. Eun, W. Park, W.H. Jang, T.-J. Kim, S.-N. Nam, Y. Yoon, S. Park, Design and applicability of a water recycling system to treat wastewater generated from real uranium-contaminated soil, Chem. Eng. J., 472 (2023) 144927.
[2] A.D. Radu, E. Panturu, A. Woinaroschy, R. Isopescu, Experimental design and process optimization for uranium polluted soils decontamination by acid washing, Water Air Soil Pollut., 226 (2015) 127.
[3] L. Chen, J. Liu, W. Zhang, J. Zhou, D. Luo, Z. Li, Uranium (U) source, speciation, uptake, toxicity and bioremediation strategies in soil-plant system: A review, J. Hazard. Mater., 413 (2021) 125319.
[4] B.-M. Jun, H.-K. Lee, S. Park, T.-J. Kim, Purification of uranium-contaminated radioactive water by adsorption: A review on adsorbent materials, Sep. Purif. Technol., 278 (2021) 119675.
[5] S.A. Darda, H.A. Gabbar, V. Damideh, M. Aboughaly, I. Hassen, A comprehensive review on radioactive waste cycle from generation to disposal, J. Radioanal. Nucl. Chem., 329 (2021) 1–17.
[6] B. Zhang, H.-Y. Sun, J. Li, L.-Z. Li, Y.-L. Deng, S.-H. Liu, M.-L. Feng, X.-Y. Huang, Fast and selective removal of aqueous uranium by a K^+-activated robust zeolitic sulfide with wide pH resistance, Inorg. Chem., 58 (2019) 11622–11629.
[7] L.M. Camacho, S. Deng, R.R. Parra, Uranium removal from groundwater by natural clinoptilolite zeolite: Effects of pH and initial feed concentration, J. Hazard. Mater., 175 (2010) 393–398.
[8] B.-M. Jun, K. Kim, J. Moon, T. Kim, D. Kim, H.-C. Eun, W. Jang, S.-N. Nam, T.-J. Kim, Y. Yoon, Design and economic comparison of uranium-contaminated soil cleaning system based on ultrasonic technology, J. Water Process. Eng., 59 (2024) 105051.
[9] B.-M. Jun, H.-H. Kim, H. Rho, J. Seo, J.-W. Jeon, S.-N. Nam, C. Min Park, Y. Yoon, Recovery of rare-earth and radioactive elements from contaminated water through precipitation: A review, Chem. Eng. J., 475 (2023) 146222.
[10] A. Boguslavsky, O. Gaskova, O. Naymushina, N. Popova, A. Safonov, Environmental monitoring of low-level radioactive waste disposal in electrochemical plant facilities in Zelenogorsk, Russia, Appl. Geochem., 119 (2020) 104598.
[11] I.-G. Kim, S.-S. Kim, G.-N. Kim, G.-S. Han, J.-W. Choi, Reduction of radioactive waste from remediation of uranium-contaminated soil, Nucl. Eng. Technol., 48 (2016) 840–846.
[12] S. Akash, B. Sivaprakash, V.C.V. Raja, N. Rajamohan, G. Muthusamy, Remediation techniques for uranium removal from polluted environment – Review on methods, mechanism and toxicology, Environ. Pollut., 302 (2022) 119068.
[13] R. Mahinroosta, L. Senevirathna, A review of the emerging treatment technologies for PFAS contaminated soils, J. Environ. Manage., 255 (2020) 109896.
[14] G. Dermont, M. Bergeron, G. Mercier, M. Richer-Laflèche, Soil washing for metal removal: A review of physical/chemical technologies and field applications, J. Hazard. Mater., 152 (2008) 1–31.
[15] L. Liu, W. Li, W. Song, M. Guo, Remediation techniques for heavy metal-contaminated soils: Principles and applicability, Sci. Total Environ., 633 (2018) 206–219.
[16] I. Kim, G.-N. Kim, S.-S. Kim, J.-W. Choi, Development of practical decontamination process for the removal of uranium from gravel, Environ. Technol., 39 (2018) 68–73.

[17] H.-K. Lee, S. Chang, W. Park, T.-J. Kim, S. Park, H. Jeon, Effective treatment of uranium-contaminated soil-washing effluent using precipitation/flocculation process for water reuse and solid waste disposal, J. Water Process. Eng., 48 (2022) 102890.
[18] S. Chang, H.-K. Lee, H.-B. Kang, T.-J. Kim, S. Park, H. Jeon, Decontamination of uranium-contaminated soil by acid washing with uranium recovery, Water Air Soil Pollut., 232 (2021) 1–10.
[19] R.I. Foster, K.-W. Kim, M.-K. Oh, K.-Y. Lee, Effective removal of uranium via phosphate addition for the treatment of uranium laden process effluents, Water Res., 158 (2019) 82–93.
[20] G.-N. Kim, S.-S. Kim, J.-K. Moon, J.-H. Hyun, Removal of uranium from soil using full-sized washing electrokinetic separation equipment, Ann. Nucl. Energy 81 (2015) 188–195.
[21] X. Zhang, P. Gu, Y. Liu, Decontamination of radioactive wastewater: State of the art and challenges forward, Chemosphere 215 (2019) 543–553.
[22] S.-A. An, J. Lee, J. Sim, C.-G. Park, J.-S. Lee, H. Rho, K.-D. Park, H.-S. Kim, Y. C. Woo, Evaluation of the advanced oxidation process integrated with microfiltration for reverse osmosis to treat semiconductor wastewater, Process Saf. Environ. Prot. 162 (2022) 1057–1066.
[23] R.H. Hailemariam, J.-S. Choi, B.A. Getachew, M.M. Damtie, H. Rho, K.-D. Park, J. Lee, Y.C. Woo, Fabrication and characterization of high-performance acetone-assisted polyamide thin-film composite membranes for fluoridated saline water treatment, Desalination 538 (2022) 115922.
[24] K. Sen, D. Mishra, P. Debnath, A. Mondal, N.K. Mondal, Adsorption of uranium (VI) from groundwater by silicon containing biochar supported iron oxide nanoparticle, Bioresour. Technol. Rep., 14 (2021) 100659.
[25] B. Zheng, J. Liao, L. Ding, Y. Zhang, W. Zhu, High efficiency adsorption of uranium in solution with magnesium oxide embedded horse manure-derived biochar, J. Environ. Chem. Eng., 9 (2021) 106897.
[26] C.-S. Lee, H. Lee, S. Sinha, A. Farsad, P. Westerhoff, H. Rho, Mini-cores of activated carbon block simulate full-sized performance for removing organics and arsenate from drinking water☆, Water Res. 267 (2024) 122461.
[27] X. Chen, J. Zhong, H. Lin, Z. Ye, Y. Wang, X. Ma, Efficient enrichment of uranium (VI) in aqueous solution using magnesium–aluminum layered double hydroxide composite phosphate-modified hydrothermal biochar: Mechanism and adsorption, Chemosphere 362 (2024) 142667.
[28] J. Liao, L. Ding, Y. Zhang, W. Zhu, Efficient removal of uranium from wastewater using pig manure biochar: Understanding adsorption and binding mechanisms, J. Hazard. Mater., 423 (2022) 127190.
[29] H. Hu, M. Gao, T. Wang, L. Jiang, Efficient uranium adsorption and mineralization recycle by nano-MgO biochar with super-hydrophilic surface, J. Environ. Chem. Eng., 11 (2023) 110542.
[30] P. Lyu, G. Wang, B. Wang, Q. Yin, Y. Li, N. Deng, Adsorption and interaction mechanism of uranium (VI) from aqueous solutions on phosphate-impregnation biochar cross-linked MgAl layered double-hydroxide composite, Appl. Clay Sci., 209 (2021) 106146.
[31] J. Liao, X. He, Y. Zhang, W. Zhu, L. Zhang, Z. He, Bismuth impregnated biochar for efficient uranium removal from solution: adsorption behavior and interfacial mechanism, Sci. Total Environ. 819 (2022) 153145.
[32] Q. Xiao, S. He, Y. Tan, K. Peng, D. Tang, X. Luo, J. Tian, G. Wang, Calcium-decorated biochar modified with phosphorus from wastewater to promote U(VI) removal: adsorption behavior and mechanism, Sep. Purif. Technol., 347 (2024) 127680.
[33] J. Liao, X. He, Y. Zhang, L. Zhang, Z. He, The construction of magnetic hydroxyapatite-functionalized pig manure-derived biochar for the efficient uranium separation, Chem. Eng. J., 457 (2023) 141367.
[34] Y. Liu, W. Yuan, W. Lin, S. Yu, L. Zhou, Q. Zeng, J. Wang, L. Tao, Q. Dai, J. Liu, Efficacy and mechanisms of δ-MnO_2 modified biochar with enhanced porous structure for uranium(VI) separation from wastewater, Environ. Pollut. 335 (2023) 122262.
[35] L. Guo, L. Peng, J. Li, W. Zhang, B. Shi, Graphitic N-doped biochar for superefficient uranium recycling from nuclear wastewater, Sci. Total Environ., 882 (2023) 163462.
[36] Y. Wang, Q. Ren, H. Xia, J. Lv, Z. Feng, C. Yin, Y. Du, Y. Li, Y. Wang, Highly efficient uranium (VI) capture by magnesium oxide loaded lotus seedpod-derived biochar via a hydrothermal and pyrolytic coupling process, Chem. Eng. Res. Des., 206 (2024) 417–427.
[37] W. Ahmed, A. Núñez-Delgado, S. Mehmood, S. Ali, M. Qaswar, A. Shakoor, D.-Y. Chen, Highly efficient uranium (VI) capture from aqueous solution by means of a hydroxyapatite-biochar nanocomposite: Adsorption behavior and mechanism, Environ. Res., 201 (2021) 111518.
[38] X. Chen, H. Xia, J. Lv, Y. Liu, Y. Li, L. Xu, C. Xie, Y. Wang, Magnetic hydrothermal biochar for efficient enrichment of uranium(VI) by embedding Fe_3O_4 nanoparticles on bamboo materials from “one-can” strategy, Colloids Surf. A: Physicochem. Eng. Asp. 658 (2023) 130748.
[39] Y. Wang, X. Wu, X. Liu, C. Cai, C. Liang, L. Dai, X. He, R. He, H. Liu, W. Zhu, Microbial etch: A novel construction method of functionalized biochar for enhanced uranium extraction in radioactive wastewater, Chemosphere 361 (2024) 142544.
[40] Y. Sun, B. Zeng, Y. Dai, X. Liang, L. Zhang, R. Ahmad, X. Su, Modification of sludge-based biochar using air roasting-oxidation and its performance in adsorption of uranium(VI) from aqueous solutions, J. Colloid Interface Sci. 614 (2022) 547–555.
[41] X. Chen, Y. Wang, H. Xia, Q. Ren, Y. Li, L. Xu, C. Xie, Y. Wang, “One-can” strategy for the synthesis of hydrothermal biochar modified with phosphate groups and efficient removal of uranium(VI), J. Environ. Radioact., 263 (2023) 107182.
[42] Y. Wang, M. Cao, Q. Peng, L. Wang, X. Cao, L. Feng, Y. Yuan, N. Wang, Polyamidoxime-loaded biochar sphere with high water permeability for fast and effective recovery of uranium from seawater, J. Water Process Eng., 55 (2023) 104205.
[43] Q. Zhou, Y. Du, Z. Feng, Q. Ren, Y. Wang, X. Chen, Y. Li, Y. Wang, Polyethyleneimine and chitosan incorporated winter melon-derived biochar composite gels for highly selective capture of uranium(VI), Colloids Surf. a: Physicochem. Eng. Asp., 699 (2024) 134719.
[44] H. Li, X. Zhang, C. Luo, H. Wang, Z. Zou, L. Liu, C. Yue, Pomelo peel derived phosphorus-doped biochar for efficient disposal of uranium-containing nuclear wastewater: Experimental and theoretical perspectives, Sep. Purif. Technol., 333 (2024) 125947.
[45] L. Dai, L. Li, W. Zhu, H. Ma, H. Huang, Q. Lu, M. Yang, Y. Ran, Post-engineering of biochar via thermal air treatment for highly efficient promotion of uranium(VI) adsorption, Bioresour. Technol., 298 (2020) 122576.
[46] T.-X. Da, H.-K. Ren, W.-K. He, S.-Y. Gong, T. Chen, Prediction of uranium adsorption capacity on biochar by machine learning methods, J. Environ. Chem. Eng., 10 (2022) 108449.
[47] Y. Zhang, B. Mei, B. Shen, L. Jia, J. Liao, W. Zhu, Preparation of biochar@chitosan-polyethyleneimine for the efficient removal of uranium from water environment, Carbohydr. Polym., 312 (2023) 120834.
[48] J. Liao, H. Chen, Y. Zhang, W. Zhu, Pyrolysis of animal manure under nitrogen atmosphere: An environment protection way to obtain animal manure biochar for high-efficient adsorption of uranium (VI), J. Anal. Appl. Pyrol., 163 (2022) 105493.
[49] S.N. Guilhen, O. Mašek, N. Ortiz, J.C. Izidoro, D.A. Fungaro, Pyrolytic temperature evaluation of macauba biochar for uranium adsorption from aqueous solutions, Biomass Bioenerg., 122 (2019) 381–390.
[50] T. Ye, B. Huang, Y. Wang, L. Zhou, Z. Liu, Rapid removal of uranium(VI) using functionalized luffa rattan biochar from aqueous solution, Colloids Surf. a: Physicochem. Eng. Asp., 606 (2020) 125480.
[51] M. Li, H. Liu, T. Chen, C. Dong, Y. Sun, Synthesis of magnetic biochar composites for enhanced uranium(VI) adsorption, Sci. Total Environ., 651 (2019) 1020–1028.
[52] S.N. Guilhen, S. Rovani, L.G.D. Araujo, J.A.S. Tenório, O. Mašek, Uranium removal from aqueous solution using macauba endocarp-derived biochar: effect of physical activation, Environ. Pollut., 272 (2021) 116022.
[53] J. Shin, J. Kwak, S. Kim, C. Son, Y.-G. Lee, S. Baek, Y. Park, K.-J. Chae, E. Yang, K. Chon, Facilitated physisorption of ibuprofen on waste coffee residue biochars through simultaneous magnetization and activation in groundwater and lake water: Adsorption mechanisms and reusability, J. Environ. Chem. Eng., 10 (2022) 107914.
[54] O. Sagi, L. Rokach, Ensemble learning: A survey, Wires Data Mining Knowl. Discov., 8 (2018) e1249.
[55] S.H. Chae, S.W. Hong, M. Son, Metadata and feature importance analyses of membrane capacitive deionization models: Is a water treatment artificial intelligence panacea possible? Desalination 585 (2024) 117784.
[56] S.H. Chae, S.W. Hong, M. Son, K.H. Cho, Determining water and solute permeability of reverse osmosis membrane using a data-driven machine learning pipeline, J. Water Process Eng., 64 (2024) 105634.
[57] S.H. Chae, S. Moon, S.W. Hong, C. Lee, M. Son, Performance investigation of osmotically assisted reverse osmosis using explainable machine learning models: A comparative study, Desalination 583 (2024) 117647.
[58] B.-M. Jun, S.H. Chae, D. Kim, J.-Y. Jung, T.-J. Kim, S.-N. Nam, Y. Yoon, C. Park, H. Rho, Adsorption of uranyl ion on hexagonal boron nitride for remediation of real U-contaminated soil and its interpretation using random forest, J. Hazard. Mater., 469 (2024) 134072.
[59] J. Shim, S. Lee, N. Yun, M. Son, S.H. Chae, K.H. Cho, Autonomous real-time control for membrane capacitive deionization, Water Res., 262 (2024) 122086.
[60] J. Sim, J. Lee, H. Rho, K.-D. Park, Y. Choi, D. Kim, H. Kim, Y.C. Woo, A review of semiconductor wastewater treatment processes: Current status, challenges, and future trends, J. Clean. Prod. 429 (2023) 139570.
[61] B.-M. Jun, S. Kim, Y. Kim, N. Her, J. Heo, J. Han, M. Jang, C.M. Park, Y. Yoon, Comprehensive evaluation on removal of lead by graphene oxide and metal organic framework, Chemosphere 231 (2019) 82–92.
[62] J. Ma, K. Fu, X. Fu, Q. Guan, L. Ding, J. Shi, G. Zhu, X. Zhang, S. Zhang, L. Jiang, Flocculation properties and kinetic investigation of polyacrylamide with different cationic monomer content for high turbid water purification, Sep. Purif. Technol., 182 (2017) 134–143.
[63] T. Pan, K. Yang, X. Dong, Y. Han, Adsorption-based capture of iodine and organic iodides: status and challenges, J. Mater. Chem. A 11 (2023) 5460–5475.
[64] L. Liu, D. Li, C. Li, R. Ji, X. Tian, Metal nanoparticles by doping carbon nanotubes improved the sorption of perfluorooctanoic acid, J. Hazard. Mater., 351 (2018) 206–214.
[65] B.-M. Jun, H.S. Hwang, J. Heo, J. Han, M. Jang, J. Sohn, C.M. Park, Y. Yoon, Removal of selected endocrine-disrupting compounds using Al-based metal organic framework: Performance and mechanism of competitive adsorption, J. Ind. Eng. Chem., 79 (2019) 345–352.
[66] S.J. Lim, J. Seo, M.G. Seid, J. Lee, W.W. Ejerssa, D.-H. Lee, E. Jeong, S.H. Chae, Y. Lee, M. Son, S.W. Hong, Clustering micropollutants and estimating rate constants of sorption and biodegradation using machine learning approaches, npj Clean Water 6 (2023) 69.
[67] D.M. Maklavany, Z. Rouzitalab, M. Bazmi, M. Askarieh, A. Nabavi-Pelesaraei, Eco-environmental analysis of different routes for the synthesis of MIL-53(Fe): An integrated life cycle assessment and life cycle cost approaches, ACS Sustain. Chem. Eng., 11 (2023) 9816–9832.

[68] A. Nabavi-Pelesaraei, H. Ghasemi-Mobtaker, M. Salehi, S. Rafiee, K.-W. Chau, R. Ebrahimi, Machine learning models of exergoenvironmental damages and emissions social cost for mushroom production, Agronomy 13 (2023) 737.
[69] H. Ghasemi-Mobtaker, F.S. Ataiee, A. Akram, A. Kaab, Feasibility study of using photovoltaic cells for a commercial hydroponic greenhouse: Energy analysis and life cycle assessment, e-Prime - Adv, Electr. Eng. Electron., 8 (2024) 100597.
[70] H. Ghasemi-Mobtaker, A. Kaab, S. Rafiee, Application of life cycle analysis to assess environmental sustainability of wheat cultivation in the west of Iran, Energy 193 (2020) 116768.